Chinese Journal of
POLYMER SCIENCE

RESEARCH ARTICLE

https://doi.org/10.1007/s10118-026-3687-5
Chinese J. Polym. Sci.

Molecularly Engineered Polyimide Films with Switchable Cavitation for Bidirectional Passive Thermal Regulation

Qiao-Ran Zhang[a*], Xin-Fei Wang[a], Ya-Nan Chen[b], Bo-Yuan Zhou[a], Hong-Liang Wei[a], Xiao-Yu Cao[a*], and Jin Wang[b*]

[a] *School of Chemistry and Chemical Engineering, Henan University of Technology, Zhengzhou 450001, China*
[b] *Key Laboratory of Multifunctional Nanomaterials and Smart Systems, Suzhou Institute of Nano-Tech and Nano-Bionics, Chinese Academy of Sciences, Suzhou 215123, China*

Electronic Supplementary Information

Abstract Passive thermal regulation materials offer a promising route toward energy-efficient building and smart devices. However, achieving both passive radiative cooling and solar-driven heating within a single polymeric system remains a significant challenge due to trade-offs in optical transparency, solar reflectivity, and environmental durability. Herein, we report a molecularly engineered polyimide (PI) film platform with switchable cavitation (realized through controlled cross-linking) that enables bidirectional thermal regulation. By tuning the molecular architecture, the PI films can be fabricated into either a highly porous, white reflective film for passive cooling (about 90% solar reflectivity, ΔT is about −6 °C) or a transparent solid film for passive heating (about 88.7% solar transmittance, ΔT is about +8 °C). The films exhibit excellent flame retardancy (PHRR is about 7.98 W·g^{-1}), thermal stability (T_{max} > 500 °C), and environmental resistance to UV and acidic conditions. Comprehensive outdoor and simulated tests confirm their dual-mode thermal regulation capabilities. This work presents a versatile strategy for designing robust, multifunctional PI materials for year-round thermal management in extreme environments, paving the way for next-generation energy-saving polymers.

Keywords Polyimide; Bidirectional thermal regulation; Passive cooling; Passive heating; Flame retardant

Citation: Zhang, Q. R.; Wang, X. F.; Chen, Y. N.; Zhou, B. Y.; Wei, H. L.; Cao, X. Y.; Wang, J. Molecularly engineered polyimide films with switchable cavitation for bidirectional passive thermal regulation. *Chinese J. Polym. Sci.* https://doi.org/10.1007/s10118-026-3687-5

INTRODUCTION

With the accelerating global demand for energy-efficient technologies, thermal regulation, particularly in buildings and wearable systems, has become a critical focus for sustainable material design. Space heating and cooling are estimated to contribute to over 50% of the total energy consumption in buildings, underscoring the urgent need for passive energy-free alternatives to conventional air conditioning and heating systems.[1–4] Passive thermal regulation technologies, including radiative cooling and solar-driven heating, hold promise owing to their intrinsic advantages such as zero energy input, minimal maintenance, and operational compatibility with both outdoor and indoor environments.

Among these strategies, passive cooling (PC) relies on materials that reflect solar radiation (0.3–2.5 μm) while emitting thermal radiation through the atmospheric transparency window (8–13 μm), achieving subambient temperatures even under direct sunlight.[5–8] Conversely, passive heating (PH) materials enable solar energy harvesting by transmitting visible light and absorbing near-infrared radiation, effectively warming enclosed spaces under cold conditions.[9–11] However, achieving both PC and PH functionalities within a single platform remains highly challenging because of their fundamentally conflicting optical design principles, that is, high solar reflectance and high transmittance.

Recent efforts to develop Janus structures, reversible phase-change materials, and stimuli-responsive coatings have led to progress in dual-mode thermal regulation.[12–19] Yet, these systems often suffer from complex fabrication processes, insufficient durability in harsh environments, and limited scalability. Notably, polymeric systems, especially those based on high-performance polymers such as polyimides (PI), offer considerable potential owing to their thermal stability, chemical resistance, optical tunability, and structural flexibility.[20–28] Conventional polyimide films are generally limited by their strong intramolecular charge transfer (CTC) interactions, which lead to high solar absorption and low transparency, thereby hindering their use in cooling or heating applications.

* Corresponding authors, E-mail: qrzhang@haut.edu.cn (Q.R.Z.)
E-mail: caoxy@haut.edu.cn (X.Y.C.)
E-mail: jwang2014@sinano.ac.cn (J.W.)
Received January 13, 2026; Accepted March 27, 2026; Published online June 26, 2026

In this context, the molecular engineering of polyimide architectures offers a new avenue for manipulating optical properties through structural design. Specifically, introducing crosslinkers into PI chains can promote phase separation and induce cavitation, leading to porous structures with strong solar scattering. In contrast, linear PIs without cross-linking exhibited dense, transparent morphologies with high visible transmittance. By tailoring the degree of cross-linking and processing conditions, it is feasible to design PI films with either white, porous architectures for passive cooling, or transparent, dense architectures for passive heating, all within a chemically robust polymer matrix.

Herein, we present a structure-tunable polyimide film system that enables bidirectional passive thermal regulation *via* controlled cavitation. By adjusting the molecular architecture through cross-linker incorporation, we prepared two types of films: (i) a porous white PI film (C-PI) that achieved about 90% solar reflectivity and a cooling effect of about 6 °C under direct sunlight, and (ii) a transparent dense PI film (CPI) that offered about 88.7% solar transmittance and a heating effect of about 8 °C. Importantly, both films demonstrated exceptional environmental stability, including UV/acid resistance, flame retardancy, and mechanical robustness, making them suitable for real-world applications. This work provides a versatile and scalable approach to designing multifunctional PI materials for year-round thermal energy modulation in demanding environments.

EXPERIMENTAL

Materials

4,4'-(Hexafluoroisopropylidene) diphthalic anhydride (6FDA) and 2,2′-bis(trifluoromethyl)-4,4′-diaminobiphenyl (TFMB) were purchased from Macklin Reagent Co., Ltd. *N*,*N*-dimethylacetamide (DMAc) was supplied by Sinopharm Chemical Reagent Company Limited. 1,3,5-tri(4-aminophenoxy) benzene (TAB) was obtained commercially from Shanghai Aladdin Technology Co., LTD. Acetic anhydride and pyridine were purchased from the Guangzhou Chemical Reagent Factory.

Fabrication of C-PI And CPI Film

Before polymerization, the dianhydride of 6FDA and diamine of TFMB diamine were dried in a vacuum oven for 12 h. The specific synthesis route was as follows: TFMB (0.8378 g, 2.6160 mmol) was added to DMAc with mechanical stirring in an ice water bath. Subsequently, 6FDA (1.1746 g, 2.6945 mmol) was added to the mixture several times with subsequent stirring for 3 h to obtain anhydride-terminated polyamic acid (PAA) oligomers. Subsequently, a cross-linker of TAB (0.1698 g, 0.4253 mmol) was slowly added into PAA with the stirring vigorously for 0.5 h, and then acetic anhydride (2.037 mL, 21.7 mmol) and pyridinium (1.748 mL, 21.7 mmol) were dropped into the mixture, obtaining cross-linking polyimide (C-PI) sol by the process of chemical imidization. The as-obtained C-PI sol was dropped onto glass substrates to achieve the desired film thicknesses (300, 400, 500, and 600 μm). Subsequently, a C-PI film-attached glass plate was placed in a fume hood to obtain a partially dried film. The resultant C-PI films were named C-PI (300 μm), C-PI (400 μm), C-PI (500 μm), and C-PI (600 μm). Similarly, a colorless polyimide (CPI) film was fabricated *via* thermal imidization according to a previous study, which is similar to the process of C-PI films without cross-linkers of TAB, acetic anhydride, and pyridinium.

Characterizations

Fourier transform infrared (FTIR) spectra of the films were recorded using a Nicolet6700 FTIR spectrophotometer (Bruker Spectrum Instruments, USA). The micromorphology of the films was observed using scanning electron microscopy (SEM; Japan Electronics, Japan). Thermogravimetric analysis (TGA, Netzsch STA 209F3, Germany) was conducted at a heating rate of 10 °C·min^{-1} under N_2 atmosphere to evaluate the thermal stability of the C-PI films, PVA, and commercial cotton. The reflective spectra (0.28–2.5 μm) of CPI and C-PI were measured by an ultraviolet–visible–near-infrared spectrometer with an integrating sphere model (ISR-3100). Fourier-transform infrared spectroscopy (FTIR) was used to record the infrared spectra of the films in the wavenumber range of 550–4000 cm^{-1}. The related infrared emittance (8–13 μm) was tested using FTIR equipment attached to a gold integrating sphere (A562, Bruker). Microcone calorimetry (MCC-2, Govmark, USA) was used to test the flame retardancy of the C-PI, PVA, and commercial cotton films. The practical thermal regulating performance was conducted at the Henan University of Technology (34°46'N,113°40'W). The experimental setup was as described in our previous study. The thermoregulation performance was evaluated using a thermal imaging camera (FLIR, E60) to record the temperature distribution of the samples.

RESULTS AND DISCUSSION

Construction and Optical Properties of Switchable Cavitation in PI Films

The preparation processes of switchable cavitation in the PI film are illustrated in (Fig. 1a), and the precursor of PAA was synthesized from dianhydride (6FDA) and diamine (TFMB). On the one hand, a porous PI film with solar scatter originating from cross-linking PI can be obtained after the incorporation of the cross-linker of TAB *via* the processes of blading, chemical imidization, and subsequent ambient pressure drying, induced by the phase separation process. A transparent CPI film with a solid structure originating from linear PI can be obtained *via* a similar process without the incorporation of TAB. It is attractive that the PI film with solar transmittance and reflection can be switched by adjusting the cross-linking structure of PI for PH and PC. As illustrated by (Fig. 1b), a switching strategy has been proposed which is based on a PI film being alternated between a transparent solid state for solar heating and a highly porous state for solar reflection by the adjusting the cross-linking structure of PI. As shown in Figs. 1(c) and 1(d), the CPI film exhibits a transparent property with a dense microstructure for permeating the solar irradiation, whereas the C-PI film shows high whiteness with a porous structure for high sunlight scattering, which is conducive to realizing PH and PC functions under various conditions by adjusting the molecular structure.

Microstructure of PI Films

The microstructure of the PI films plays an important role in determining their spectral characteristics.[29–31] Therefore, the microstructure of the as-prepared C-PI films with various designed thickness (300–600 μm) was observed by scanning electron microscope (SEM), and the related SEM images of C-PI are shown

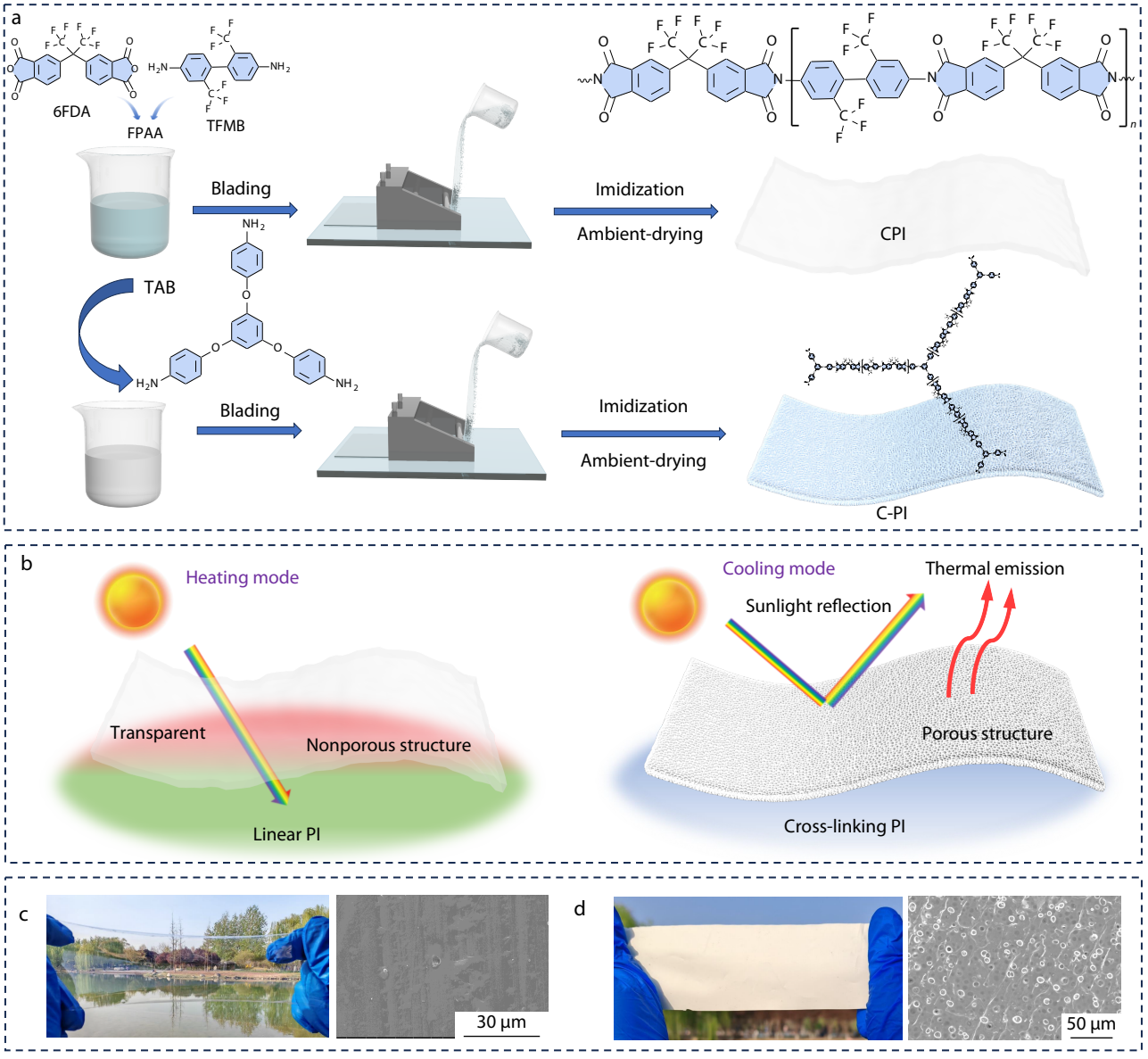

Fig. 1 Preparation and design of PI films. (a) Schematic of the preparation process of CPI and C-PI films; (b) Schematic illustration of CPI film for passive heating and C-PI film for passive cooling; Digital pictures and SEM images of the surface of (c) CPI and (d) C-PI film.

in (Figs. 2a–2d), it could be well observed that C-PI films exhibit similar 3D porous structure with micrometer scales, contributing to enhance the solar scatter to realize high sunlight reflectivity. In addition, the resultant C-PI film exhibited low weight, superior fire resistance, and flexibility, as shown in Fig. S1 (in the electronic supplementary information, ESI).

The mechanical properties of the resultant films are shown in Fig. 2(e) and Fig. S2 (in ESI), and the corresponding moduli are summarized in (Fig. 2f). By analyzing the related tensile stress-strain curves of the C-PI films in (Fig. 2e), it can be concluded that the tensile strength of C-PI is superior to that of the CPI film, indicating that the cross-linked structure contributes to enhancing the tensile strength resulting from the enhanced molecular skeleton. In addition, C-PI (400 μm) exhibited the highest tensile strength (about 13.3 MPa) at a strain of 9.6%, indicating its superior mechanical properties. The comparison of their moduli also indicates a higher modulus (about 279.6 MPa) for C-PI (400 μm), further confirming its outstanding mechanical performance. The high mechanical strength mainly results from the highly cross-linked structure with irreversible properties. The porosities of the various C-PI films are summarized in (Fig. 2g), reflecting the porous structure of the C-PI films for solar scattering.

The statistical distributions of the porous diameters of the various C-PI films are shown in (Fig. 2h) and (Figs. S3–S5a in ESI), and the corresponding FDTD simulation results for the scattering efficiencies are presented in Fig. 2(i) and Figs. S3–S5(b) (in ESI). The porous diameter of the C-PI films is mainly distributed in the range of 3–10 μm, which enhances the solar scattering efficiency. The related FDTD simulation results further demonstrate the strong Mie scatter efficiency of the C-PI film to strongly reflect sunlight owing to the ap-

https://doi.org/10.1007/s10118-026-3687-5

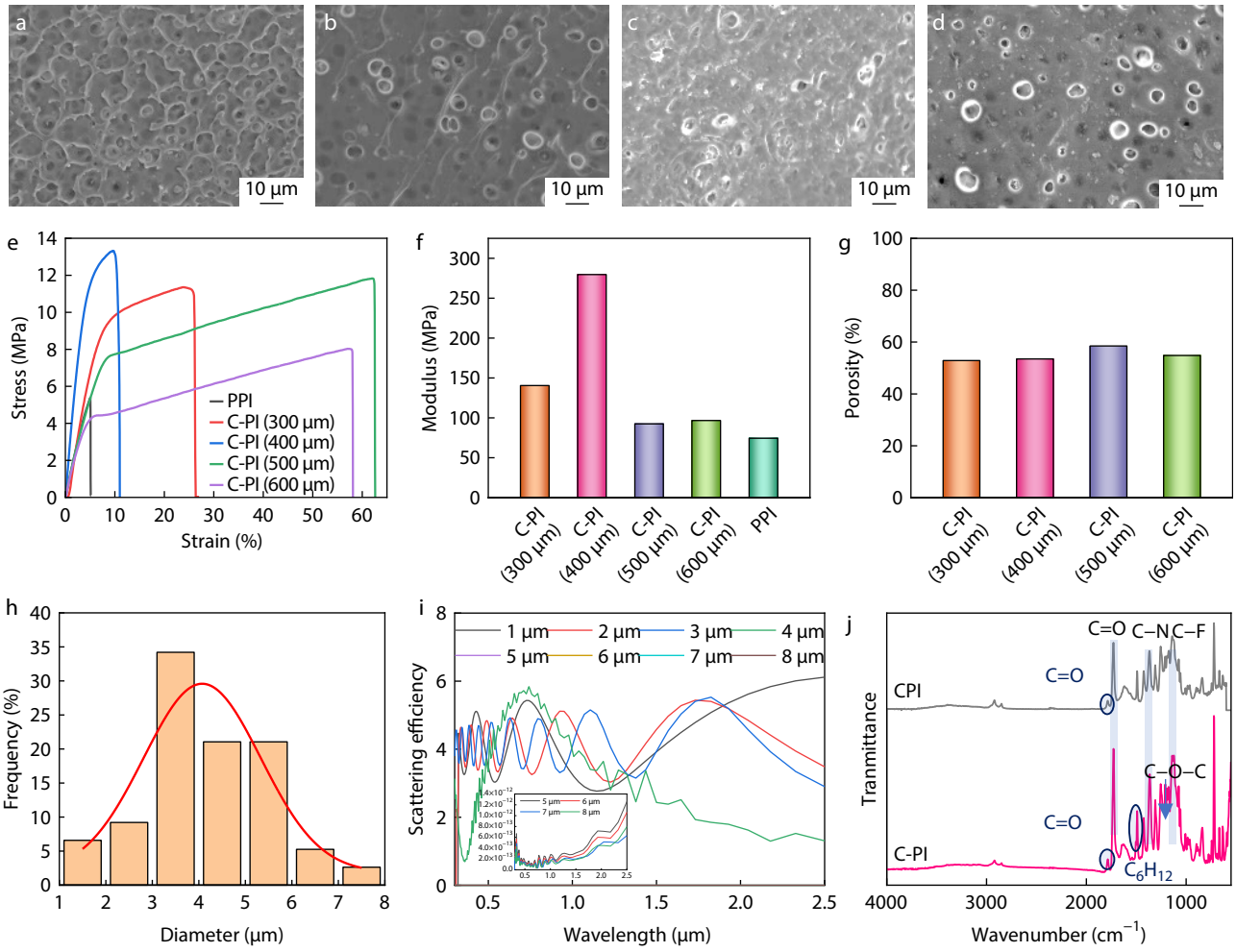

Fig. 2 The morphology and microstructure of C-PI films. (a–d) SEM image of the surface of various C-PI films from 300–600 μm; (e) Tensile stress-strain curves, (f) modulus and (g) porosity of PI films. (h) Statistical distribution of the porous diameter and (i) FDTD simulation results of the scattering efficiencies of C-PI; (j) FTIR spectra of the films.

propriate porous size, especially centered at 3–5 μm. Based on these analyses, the C-PI (400 μm) film was selected as the most representative sample, denoted as C-PI, for further research and discussion. Moreover, as shown (Fig. 2j), CPI and C-PI both have asymmetric C=O (1783 cm^{-1}), symmetric stretching vibrations C=O (1716 cm^{-1}), and a stretching vibration peak C—N (1354 cm^{-1}) in the FTIR spectrum, confirming the presence of imide rings in PI.[32–35] And the C—F bond (1128 cm^{-1}) reflects the successful incorporation of a fluorine-containing group into PI.[36,37] C-PI presented new bonds of the benzene ring (1450–1600 cm^{-1}) and C—O—C (1250–1150 cm^{-1}), indicating the successful incorporation of TAB into PI.[38]

Physical Properties and Fire Resistance of PI Films

Mechanical properties and fire resistance are key performance factors for film applications. As shown in (Fig. 3a), the as-obtained C-PI film was white and could be folded and twisted for 1000 cycles, presenting good flexibility. The mechanical properties of the C-PI films before and after folding were compared, and the corresponding tensile strain-stress curves and modulus results are shown in (Figs. 3b and 3c), respectively. It can be concluded that the tensile strength and modulus were well maintained after 1000 cycles, demonstrating its outstanding flexibility and high mechanical properties. In addition, as shown in (Fig. 3d), the resultant film can withstand a weight of 50 kg without any damage or breakage, presenting huge potential in practical applications. Moreover, the fire resistance of C-PI and other thermoregulating textiles such as poly(vinyl alcohol) (PVA) and commercial cotton was evaluated. All samples were ignited using butane, and the combustion phenomenon was recorded. PVA and commercial cotton combusted violently, exhibiting poor fire resistance. In contrast to PVA and commercial cotton, the C-PI film undergoes a self-extinguishing phenomenon quickly after ignition, which can effectively resist high-temperature fires.

Microcone calorimetry tests were conducted to further evaluate the flame retardancy of the composites.[39,40] The heat release rate (HRR) and total heat release (THR) curves of C-PI, PVA, and commercial cotton are shown in (Figs. 3e and 3f), respectively. The related peak values are summarized in (Figs. 3g and 3h). PVA and commercial cotton both exhibited higher peak heat release rate (PHRR) values of 152 and 174 $W \cdot g^{-1}$, respectively, reflecting their potential fire hazards. In

https://doi.org/10.1007/s10118-026-3687-5

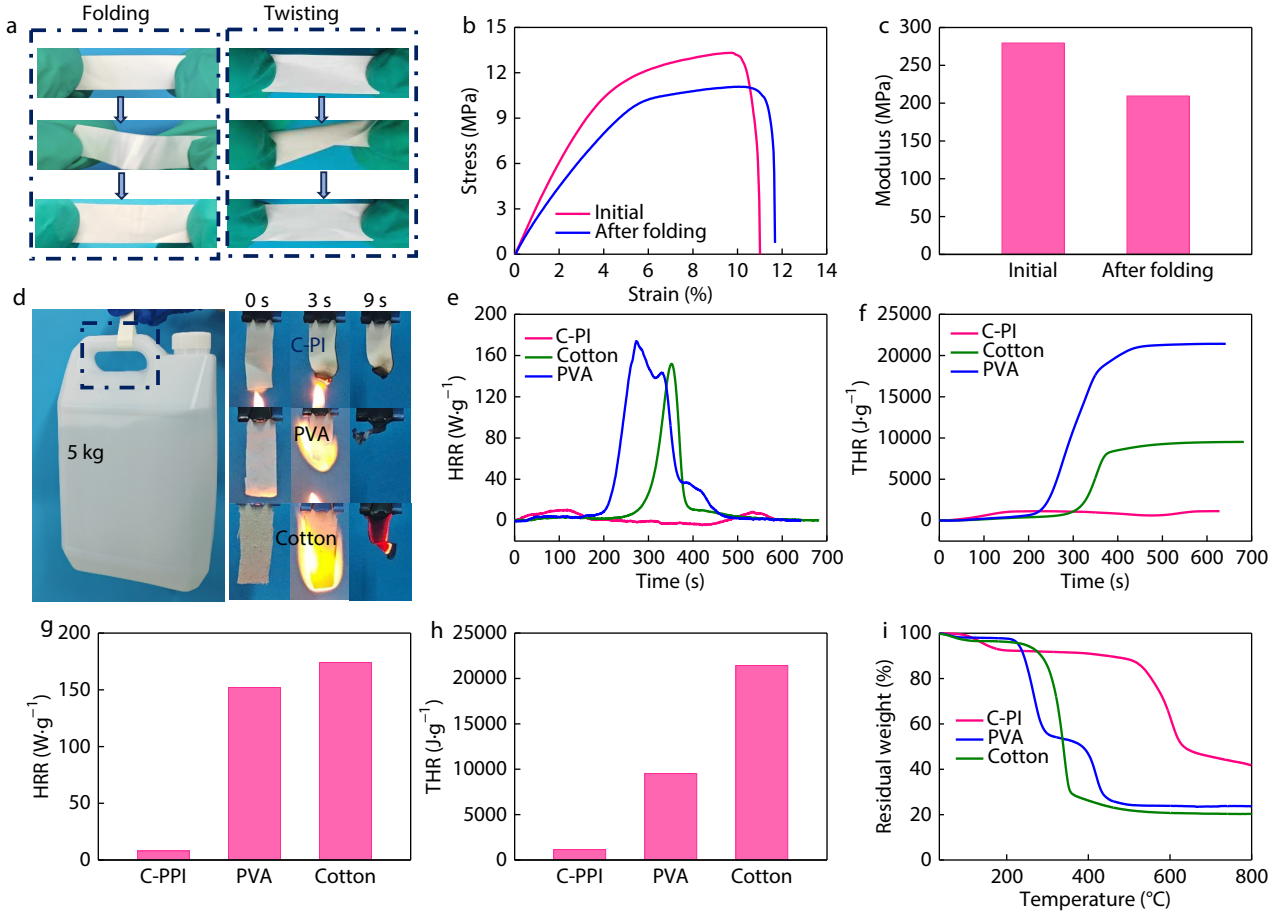

Fig. 3 Flame retardancy and mechanical properties of C-PI films. (a) Optical pictures of C-PI films before and after folding/twisting for 1000 cycles; (b) Tensile stress-strain curves as well as (c) modulus of C-PI films before and after folding for 1000 cycles; (d) Optical pictures of C-PI films with loading of weight with 5 kg and by igniting by butane; (e) HRR and (f)THR curves of C-PI, PVA, and commercial cotton; The comparison of (g) HRR and (h) THR values among C-PI, PVA, and commercial cotton; (i) The thermogravimetric curves of C-PI, PVA, and commercial cotton.

contrast to PVA and commercial cotton, C-PI presented PHRR values as low as 7.98 $W \cdot g^{-1}$, demonstrating its superior fire resistance. THR value still presents the similar trend that PVA and cotton exhibit high values of 9523.3 $J \cdot g^{-1}$ and 21421.5 $J \cdot g^{-1}$, respectively, while that of C-PI is just 1129.9 $J \cdot g^{-1}$. The TGA curves of the different samples are depicted in (Fig. 3i), which show the highest maximum thermal decomposition temperature of our films, demonstrating its outstanding thermal stability. The ideal mechanical strength, thermal stability, and outstanding flame retardancy of our C-PI film are conducive to its high stability in harsh practical environments.

Environmental Stability of PI Films

The IR thermal images of the C-PI film and commercial cotton under irradiation by a solar simulator are shown in (Fig. 4a), and the related temperature difference between the samples and background is shown in (Fig. 4b), for further evaluation of the PC performance. The results revealed that the C-PI film had a lower surface temperature than commercial cotton, confirming its superior cooling effectiveness. A comparison of the temperature difference data between them can also reveal their superior cooling performance. To the best of our knowledge, high environmental stability involving UV and acid resistance of thermoregulating materials is also a key indicator for practical applications.[41–43] (Figs. 4c and 4d) provide digital pictures of our films before and after UV and acid treatment to evaluate the UV/acid resistance. No obvious changes were observed before and after the treatment, demonstrating excellent environmental stability. The solar reflective spectra of the films before and after treatment are also shown in (Figs. 4e and 4f), showing that they can well resist UV and acid according to the good anastomosis curves before and after treatment. SEM images of the C-PI film after acid treatment, UV exposure, and outdoor exposure are shown in (Figs. S6–S8 in ESI) and the pore structure was stable after various aging treatments, further demonstrating its environmental stability. The FTIR spectra of the C-PI films after acid treatment, UV exposure, and outdoor exposure are presented in Fig. S9 (in ESI), and their chemical structures did not undergo significant changes, confirming their excellent stability. In addition, the resultant film exhibited self-cleaning properties, which are conducive to durable thermal regulation in outdoor environments (Fig. S10 in ESI).

As shown in (Fig. 4g), the C-PI film presents superior advantages over other PC materials, such as higher solar reflectivity, lower PHRR, and char residue value.[44–48] The comparison of sunlight reflectance and tensile strength among the resultant films and other types of PC materials is shown in (Fig. 4h), fur-

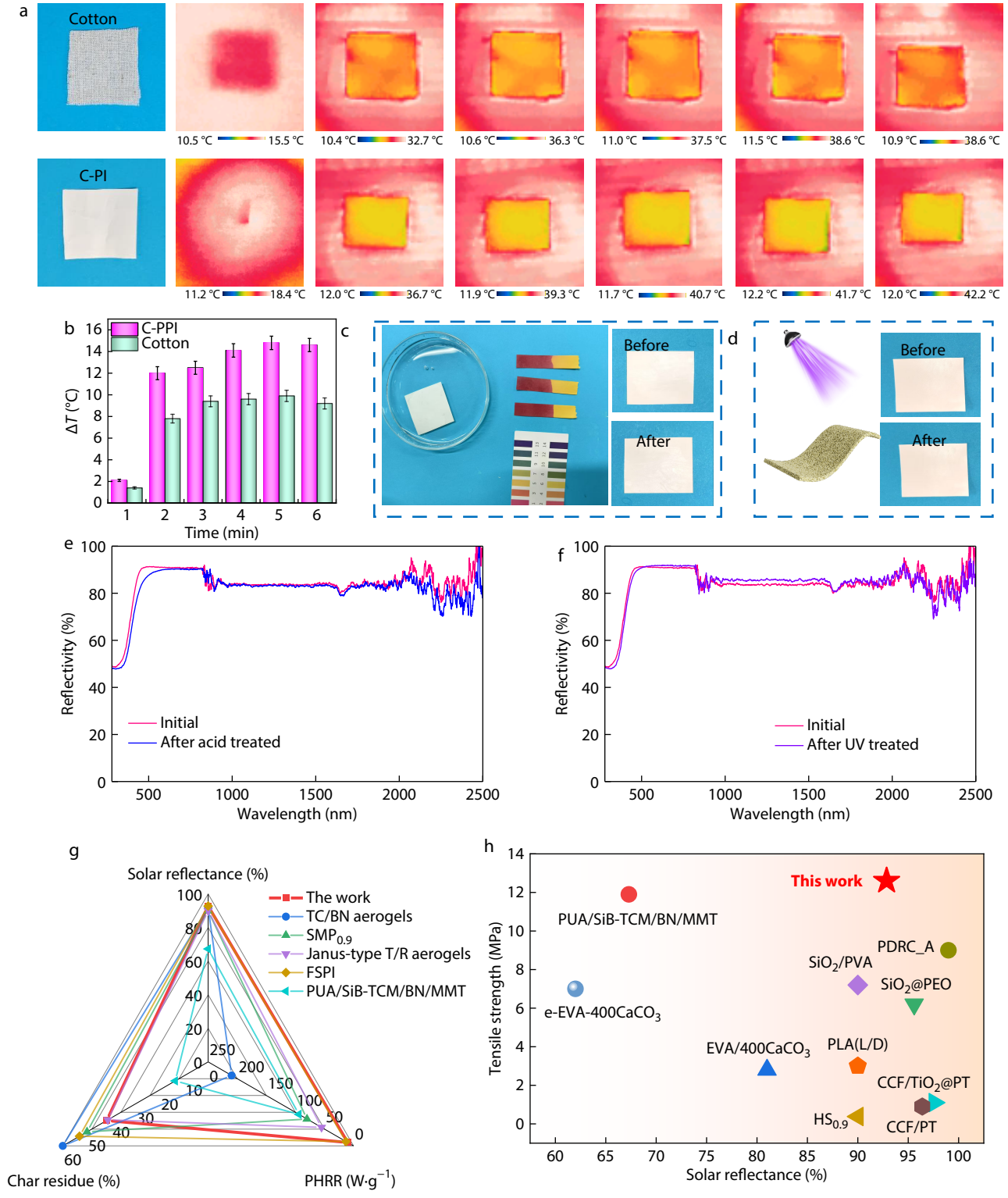

Fig. 4 Environmentally stability of C-PI films. (a) Optical and infrared images of C-PI with the irradiation by solar simulator; (b) Temperature differences between the surface temperature of samples and the background; (c) The optical images of the film before and after being soaked in an acidic solution for 48 h; (d) Optical images of the film before and after being exposed under UV lamp for 24 h; (e) Sunlight reflectance of PPI film before and after acidic solutions treatment; (f) Sunlight reflectance of the film before and after acidic solutions treatment UV treatment; (g) Comparison of the comprehensive performances involving the sunlight reflectivity, PHRR, and char residue between the film and other PC materials reported in the literature; (h) The comparison of tensile strength and sunlight reflectivity between the film and other PC materials according to the literature.

https://doi.org/10.1007/s10118-026-3687-5

ther demonstrating the desirable high mechanical strength and optical properties of this work. [44,47,49–56]

Practical Thermoregulating Performance of PI Films

The optical properties of the solar spectrum (0.3–2.5 μm) of CPI and C-PI films in the solar spectrum are shown in (Figs. 5a–5c). The C-PI film with a porous structure could reflect about 90.0% solar radiation (Fig. 5a) and allow for about 94% mid-infrared (MIR) thermal emittance (Fig. S11 in ESI), while the transparent CPI film exhibited a transmittance of about 88.7% in the visible band of the solar spectrum (Fig. 5c). In addition, the CIE chromaticity coordinate (Fig. 5b) analysis can also demonstrate the high whiteness of the C-PI film, which is consistent with its related optical pictures. The desired optical property of the C-PI film with high sunlight reflectivity endows it with the desired PC performance, whereas the CPI film with high solar transparency characteristics contributes to the realization of PH effectivity.

Thus, the outdoor thermoregulating performances of the CPI and C-PI films were tested in Zhengzhou (China) on February 23, 2025, utilizing the self-constructed setup. The related schematic and digital picture of the setup are shown in Figs. 5(d) and 5(e), respectively. The real irradiation and temperature-time curves in the practical tests on a clear day are shown (Figs. 5f and 5g), respectively. The C-PI film presents (Fig. 5g) cooling efficiency with a maximum temperature reduction of about 6.1 °C while CPI film shows solar heating

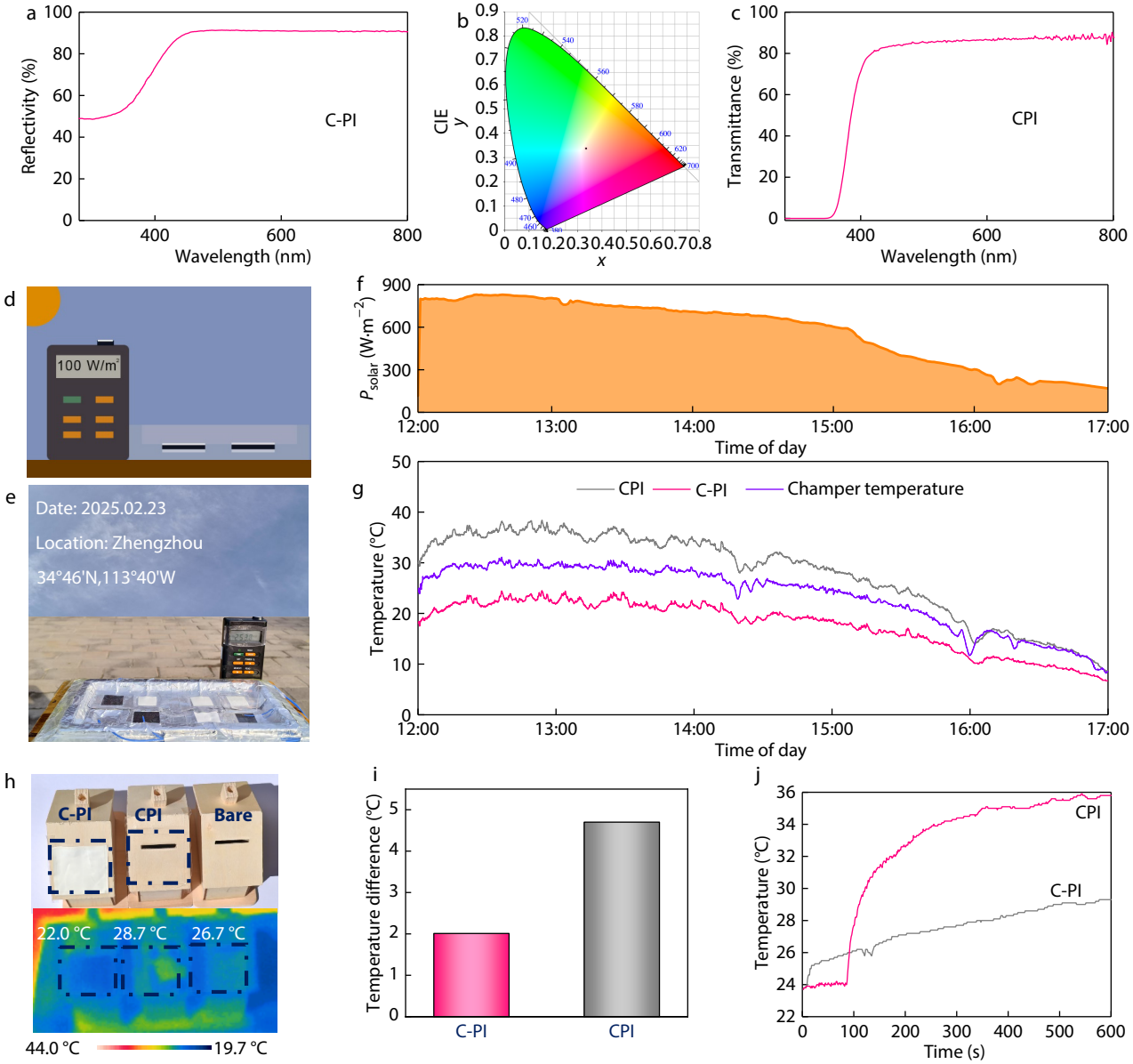

Fig. 5 Outdoor daytime thermal management performance of the C-PI and CPI films. (a) Solar reflectivity as well as (b) CIE chromaticity coordinates of C-PI film.; (c) Solar transmittance of CPI film; (d) Schematic diagram and (e) optical picture of the temperature measurement setup; (f) Solar irradiation and (g) real-time temperature in Zhengzhou, China (February 23, 2025); (h) Digital and infrared images of the bare house model as well as covered by C-PI and CPI films under irradiation by a solar simulator; (i) The temperature differences between the samples and bare house; (j) The temperature-time curves of C-PI and CPI films under irradiation by the solar simulator measured by thermoelectric couple.

https://doi.org/10.1007/s10118-026-3687-5

performance with a maximum temperature increasement of about 8.5 °C during periods of about 700 W·m^{-2} solar intensity (I_{solar}) from 12:00 to 17:00. In addition, the C-PI film presented a higher radiative cooling power with a peak value of 120.15 W·m^{-2} and its potential cooling energy savings when applied to a building's exterior surfaces (roof and walls) are shown in Figs. S12(a) and S12(b) (in ESI). The results confirmed the higher radiative cooling capacity of the as-obtained C-PI film with a porous structure as well as the heating performance with high visible transparent characteristics, which are expected to emerge as candidates for next-generation passive thermoregulating performance.

The house models covered by the C-PI film and CPI film were directly exposed to a solar simulator in which the temperature distribution was recorded by an infrared camera (Fig. 5h) to further measure the thermoregulating performances of the resultant films. Compared to bare house model, CPI film exhibited heating performance with an enhanced temperature of about 2.0 °C while the C-PI film exhibited cooling performance with about 4.7 °C decreasing temperature, which can be also evident from the related temperature difference between CPI and C-PI film with bare house recorded in (Fig. 5i). The real-time temperatures of the films under the irradiation of the solar simulator are shown in (Fig. 5j). After irradiation for 600 s, CPI film exhibited an equilibrium temperature of about 36 °C while C-PI film presents about 28.5 °C, and the obvious temperature difference between them was well consistent with the results mentioned, confirming their opposite thermal management effects on cooling and heating performance.

CONCLUSIONS

In summary, we developed a structure-engineered polyimide (PI) film platform capable of bidirectional passive thermal regulation through tunable cavitation control. By modulating the molecular architecture *via* cross-linking, the system yielded either a porous white film (C-PI) with about 90% solar reflectivity for radiative cooling (ΔT is about –6 °C) or a transparent dense film (CPI) with about 88.7% solar transmittance for solar-driven heating (ΔT is about +8 °C). This functionality was achieved through a scalable and controllable fabrication strategy involving phase separation and chemical imidization. Beyond dual-mode thermal management, the films exhibited excellent flame retardancy, mechanical robustness, and resistance to UV and acidic environments, enabling reliable performance under harsh outdoor conditions. This work demonstrates a versatile molecular design strategy for thermal regulation *via* cavity control, offering a promising path toward next-generation energy-efficient polymeric materials for buildings, thermal textiles, aerospace insulation, and other applications that require adaptive thermal modulation.

Conflict of Interests

The authors declare no interest conflict.

Electronic Supplementary Information

Electronic supplementary information (ESI) is available free of charge in the online version of this article at http://doi.org/10.1007/s10118-026-3687-5.

Data Availability Statement

The data that support the findings of this study are available from the corresponding author upon reasonable request.

ACKNOWLEDGMENTS

This work was financially supported by the Natural Science Foundation of Henan Province (No. 252300421539), High-level Talent Funds of Henan University of Technology (No. 2023BS067), Key Science and Technology Project of Henan Province (No. 252102231061), Horizontal project (No. 098H2024HG098), and Basic Research Program of Jiangsu Province (No. BK20240027).

REFERENCES

1 Huang, G.; Yengannagari, A. R.; Matsumori, K.; Patel, P.; Datla, A.; Trindade, K.; Amarsanaa, E.; Zhao,T.; Kohler, U.; Busko, D. Richards, B. S. Radiative cooling and indoor light management enabled by a transparent and self-cleaning polymer-based metamaterial. *Nat. Commun.* **2024**, *15*, 3798.
2 Jing, C.; Wang, T.; Zhang, J.; Ma, J.; Cheng, J. Cheng, Superhydrophobic, superoleophobic, robust and sprayable radiative cooling nanocomposites *via* multifluorination and multilevel interfacial regulation strategy. *Adv. Funct. Mater.* **2025**, *35*, 2422260.
3 Yu, H.; Lu, J.; Yan, J.; Bai, T.; Niu, Z.; Ye, B.; Cheng, W.; Wang, D.; Huan, S.; Han, G.; Selective emission fabric for indoor and outdoor passive radiative cooling in personal thermal management. *Nano-Micro. Lett*. **2025**, *17*, 192.
4 Liu, C.; Xue, T.; Yang, Y.; Mu, X.; Wan, X.; Fan, W.; Liu, T. Shape memory polyimide aerogel fabrics with high-thermal-switching-ratio enabled by synergistic micro-and macro-deformation. *Adv. Funct. Mater*. **2026**, e30874.
5 Li, D.; Liu, X.; Li, W.; Lin, Z.; Zhu, B.; Li, Z.; Li, J.; Li, B.; Fan, S.; Xie, J.; Zhu, J. Scalable and hierarchically designed polymer film as a selective thermal emitter for high-performance all-day radiative cooling. *Nat. Nanotechnol.* **2021**, *16*, 153.
6 Song, Y. N.; Li, Y.; Yan, D. X.; Lei, J.; Li, Z. M. Novel passive cooling composite textile for both outdoor and indoor personal thermal management. *Compos. Part. A-Appl. S.* **2020**, *130*, 105738.
7 Shan, X.; Liu, L.; Wu, Y.; Yuan, D.; Wang, J.; Zhang, C.; Wang, J. Aerogel-functionalized thermoplastic polyurethane as waterproof, breathable freestanding films and coatings for passive daytime radiative cooling. *Adv. Sci.* **2022**, *9*, 2201190.
8 Xue, T.; Zhu, C.; Feng, X.; Wali, Q.; Fan, W.; Liu, T. Polyimide aerogel fibers with controllable porous microstructure for super-thermal insulation under extreme environments. *Adv. Fiber. Mater.* **2022**, *4*, 1118–1128.
9 Li, K.; Chang, T. H.; Li, Z.; Yang, H.; Fu, F.; Li, T.; Ho, J.S. Biomimetic MXene textures with enhanced light-to-heat conversion for solar steam generation and wearable thermal management. *Adv. Energy. Mater.* **2019**, *9*, 1901687.
10 Zhao, L.; Bhatia, B.; Yang, S.; Strobach, E.; Weinstein, L. A.; Cooper, T. A.; Chen, G.; Wang, E.N. Harnessing heat beyond 200 °C from unconcentrated sunlight with nonevacuated transparent aerogels. *ACS Nano* **2019**, *13*, 7508.
11 Wang, J.; Shan, X.; Hu, P.; Zhang, C.; Yuan, D.; Hu, X.; Wang, J.

Graphical Abstract

Molecularly Engineered Polyimide Films with Switchable Cavitation for Bidirectional Passive Thermal Regulation

Qiao-Ran Zhang, Xin-Fei Wang, Ya-Nan Chen, Bo-Yuan Zhou, Hong-Liang Wei, Xiao-Yu Cao, and Jin Wang

Henan University of Technology; Suzhou Institute of Nano-Tech and Nano-Bionics, Chinese Academy of Sciences

Structure-tunable polyimide films enable radiative cooling (about 90% reflectivity, ΔT is about −6 °C) and solar heating (about 88.7% transmittance, ΔT is about +8 °C), while offering flame retardancy, thermal stability, and UV/acid resistance.

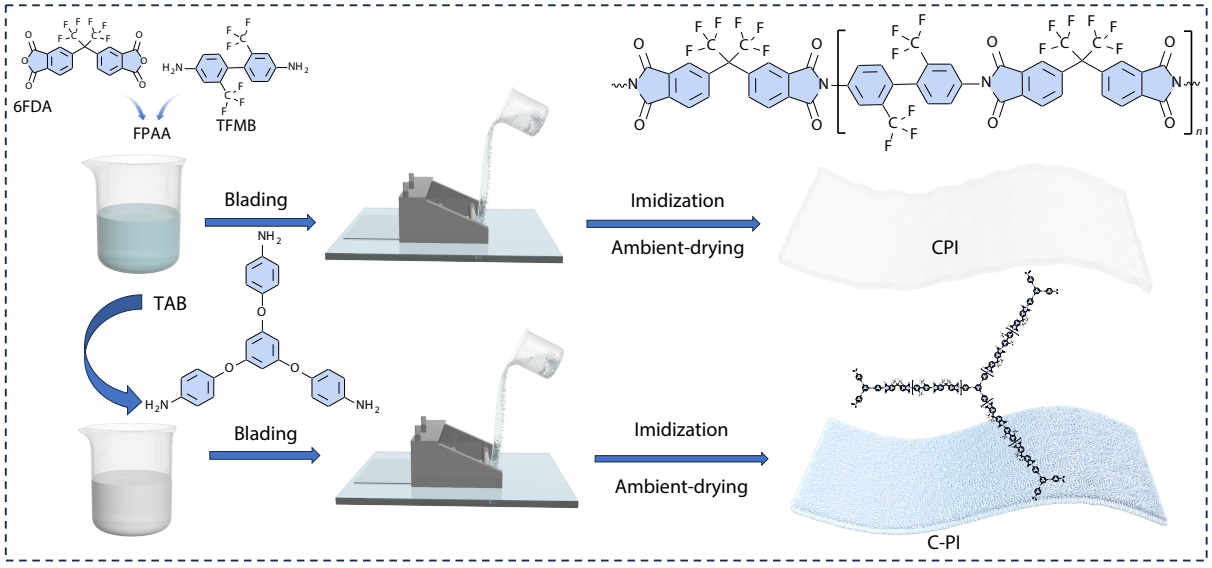

Chinese J. Polym. Sci., 2026 *https://doi.org/10.1007/s10118-026-3687-5*

Bioinspired multilayer structures for energy-free passive heating and thermal regulation in cold environments. *ACS Appl. Mater. Interfaces* **2022**, *14*, 46569−46580.

12 Ni, Y.; Li, B.; Chu, C.; Wang, S.; Jia, Y.; Cao, S.; Neisiany, R.E.; He, C.; Chen, S.; You, Z. One-step fabrication of ultrathin porous Janus membrane within seconds for waterproof and breathable electronic skin. *Sci. Bull.* **2025**, *70*, 712−721.

13 Miao, D.; Cheng, N.; Wang, X.; Yu, J.; Ding, B. Sandwich-Structured textiles with hierarchically nanofibrous network and Janus wettability for outdoor personal thermal and moisture management. *Chem. Eng. J.* **2022**, *450*, 138012.

14 Li, Y.; Zhang, X. Electrically conductive, optically responsive, and highly orientated Ti_3C_2Tx MXene aerogel fibers. *Adv. Funct. Mater.* **2021**, *32*, 2107767.

15 Zhou, X.; Ge, J.; Yang, X.; Yang, Q.; Feng, Y.; Feng, W. Phase-change gradient composites for variable thermal management. *Compos. Commun.* **2024**, *48*, 101948.

16 Dai, B.; Li, X.; Xu, T.; Zhang, X. Radiative cooling and solar heating janus films for personal thermal management. *ACS Appl. Mater. Interfaces* **2022**, *14*, 18877.

17 Catrysse, P. B.; Song, A. Y.; Fan, S. Photonic structure textile design for localized thermal cooling based on a fiber blending scheme. *ACS Photonics* **2016**, *3*, 2420.

18 Cao, Z.; Zhang, S.; Wang, C.; Xu, Y.; Zhao, W.; Li, X.; Zhang, Y. , Cui, Z.; Fu, P.; Pang, X.; Zhang, X.; Liu, M.; Reactive extrusion for efficient preparation of high temperature resistant PA6T/66/BN composites with great thermal management and mechanical properties. *Compos. Commun.* **2024**, *52*, 102121.

19 Niu, H.; Zhang, K.; Xiao, G.; Yao, Y. Vertically interconnected structure enhances the thermal management capability of copper-based composites. *Compos. Commun.* **2024**, *48*, 101906.

20 Liu, X.; Zhang, H.; Pan, Y.; Ma, J.; Liu, C.; Shen, C. A transparent polymer-composite film for window energy conservation. *Nano-Micro. Lett.* **2025**, *17*, 151.

21 Li, Q.; Guo, Y.; Yi, S.; Xu, Z.; Duan, W.; & Liu, S. Fluorinated polyimide/sepia eumelanin nanocomposites for aerospace applications. *ACS Appl. Polym. Mater.* **2023**, *5*, 1520.

22 Li, Q.; Sun, Y.; Zhou, B.; Han, G.; Feng, Y.; Liu, C.; & Shen, C. Flexible, stretchable, and transparent MXene nanosheet/thermoplastic polyurethane films for multifunctional heating and electromagnetic interference shielding. *ACS Appl. Nano. Mater.* **2023**, *6*, 3395.

23 Vivod, S. L.; Meador, M. A. B.; Pugh, C.; Wilkosz, M.; Calomino, K.; McCorkle, L. McCorkle, Toward improved optical transparency of polyimide aerogels. *ACS Appl. Mater. Interfaces* **2020**, *12*, 8622.

24 Zhang, Q.; Xue, T.; Lu, Y.; Ma, L.; Yu, D.; Liu, T.; Fan, W. Fluorine-containing polyimide nanofiber membranes for durable and anti-aging daytime radiative cooling. *J. Mater. Sci. Technol.* **2024**, *179*, 166.

25 Zhang, Q.; Wang, T.; Du, R.; Zheng, J.; Wei, H.; Cao, X.; Liu, X.

Highly stable polyimide composite nanofiber membranes with spectrally selective for passive daytime radiative cooling. *ACS Appl. Mater. Interfaces* **2024**, *16*, 40069.
26 Song, X.; Gong, H.; Li, H.; Zhang, M.; Jiang, L.; Wang, C.; Jiang, P.; Wang, H.; Cao, K.; Liu, G.; Zhao, Q.; Fan, T.; Molecularly and structurally designed polyimide nanofiber radiative cooling films for spacecraft thermal management. *Adv. Funct. Mater.* **2024**, *35*, 2413191.
27 Zhao, H.; Sun, Q.; Zhou, J.; Deng, X.; Cui, J. Switchable cavitation in silicone coatings for energy-saving cooling and heating. *Adv. Mater.* **2020**, *32*, 2000870.
28 Luo, B.; Liang, X.; Ruan, H.; Li, Y.; Wen, Z. Bioinspired asymmetric porous natural rubber films: wearables for electromagnetic shielding, fetal monitoring, and personal thermal management. *Adv. Funct. Mater.* **2026**, *36*, e21742.
29 Liu, J.; Wei, Y.; Zhong, Y.; Zhang, L.; Wang, B.; Feng, X.; Xu, H.; Mao, Z. Hierarchical gradient structural porous metamaterial with selective spectral response for daytime passive radiative cooling. *Adv. Funct. Mater.* **2024**, *34*, 2406393.
30 Tang, W.; Zhan, Y.; Yang, J.; Meng, X.; Zhu, X.; Li, Y.; Lin, T.; jiang, L.; Zhao, Z.; Wang, S. Cascaded heteroporous nanocomposites for thermo-adaptive passive radiation cooling. *Adv. Mater.* **2024**, *36*, 2310923.
31 Liu, L.; Yuan, D.; Hu, X.; Hu, P.; Wang, J.; Li, Q. Wind-proof and moisture permeability aerogel-functionalized textile as all-seasonal passive thermal regulators. *Adv. Funct. Mater.* **2024**, *34*, 2411551.
32 Gu, W.; Wang, G.; Zhou, M.; Zhang, T.; Ji, G. Polyimide-based foams: fabrication and multifunctional applications. *ACS Appl. Mater. Interfaces* **2020**, *12*, 48246.
33 Zhao, X.; Yang, F.; Wang, Z.; Ma, P.; Dong, W.; Hou, H.; Fan, W.; Liu, T. Mechanically strong and thermally insulating polyimide aerogels by homogeneity reinforcement of electrospun nanofibers. *Compos. Part B: Eng.* **2020**, *182*, 107624.
34 Xue, T.; Fan, W.; Zhang, X.; Zhao, X.; Yang, F.; Liu, T. Layered double hydroxide/graphene oxide synergistically enhanced polyimide aerogels for thermal insulation and fire-retardancy. *Compos. Part. B. Eng.* **2021**, *219*, 108963.
35 Hou, X.; Zhang, R.; Fang, D. Polyimide aerogel membranes with adjustable transparency and high flexibility for highly efficient solar thermal collection. *ACS Sustain. Chem. Eng.* **2021**, *9*, 7638.
36 Shi, T.; Jing, J.; Qian, Z.; Wu, G.; Tian, G.; Liu, H.; Wang, X. Wang, Sandwich-structured fluorinated polyimide aerogel/paraffin phase-change composites simultaneously enables gradient thermal protection and electromagnetic wave transmission. *Adv. Sci.* **2025**, *12*, 2411758.
37 Lan, Z.; Li, C.; Yu, Y.; Wei, J. Colorless semi-alicyclic copolyimides with high thermal stability and solubility. *Polymers* **2019**, *11*, 1319.
38 Feng, J.; Wang, X.; Jiang, Y.; Du, D.; Feng, J. Feng, Study on thermal conductivities of aromatic polyimide aerogels. *ACS Appl. Mater. Interfaces* **2016**, *8*, 12992.
39 Hou, Y.; Chu, F.; Ma, S.; Hu, Y.; Hu, W.; Gui, Z. Rapid synthesis of oxygen-rich covalent C_2N (CNO) nanosheets by sacrifice of HKUST-1: Advanced metal-free nanofillers for polymers. *ACS Appl. Mater. Interfaces* **2018**, *10*, 32688.
40 Hou, Y.; Qiu, S.; Hu, Y.; Kundu, C. K.; Gui, Z.; Hu, W. Construction of bimetallic ZIF-derived Co–Ni LDHs on the surfaces of GO or CNTs with a recyclable method: toward reduced toxicity of gaseous thermal decomposition products of unsaturated polyester resin. *ACS Appl. Mater. Interfaces* **2018**, *10*, 18359.
41 Song, J.; Shen, Q.; Shao, H.; Deng, X. Anti-environmental aging passive daytime radiative cooling. *Adv. Sci.* **2024**, *11*, 2305664.
42 Li, Z.; Chen, Q.; Song, Y.; Zhu, B.; & Zhu, J. Fundamentals, materials, and applications for daytime radiative cooling. *Adv. Mater. Technol.* **2020**, *5*, 1901007.
43 Yao, P.; Chen, Z.; Liu, T.; Liao, X.; Yang, Z.; Li, J.; Jiang, Y.; Xu, N.; Li, W.; Zhu, B.; Zhu, J. Spider-silk-inspired nanocomposite polymers for durable daytime radiative cooling. *Adv. Mater.* **2022**, *34*, 2208236.
44 Cai, W.; Qi, L.; Cui, T.; Lin, B.; Rahman, M. Z.; Hu, X.; Ming, Y.; Chan, A.; Xing, W.; Wang, D.; Fei, B.; Fan, J. Chameleon-inspired, dipole moment-increasing, fire-retardant strategies toward promoting the practical application of radiative cooling materials. *Adv. Funct. Mater.* **2025**, *35*, 2412902.
45 Zhang, Q.; Wang, X.; Hu, X.; Yang, D.; Wei, H.; Cao, X.; Hou, Y.; Wang, J. Green synthesis of fluorine-containing polyimide aerogels toward passive daytime radiative cooling for energy saving. *Compos. Commun.* **2025**, *57*, 102450.
46 Cai, W.; Li, Z.; Xie, H.; Wang, W.; Cui, T.; Lin, B.; Qi, L.; Hu, X.; Du, Y.; Ming, Y.; Shi, S.; Chen, D.; Fei, B.; Xing, W.; Hu, Y. Thermally managed and fireproof composite aerogels for safer and year-round energy saving. *Chem. Eng. J.* **2024**, *483*, 149006.
47 Pan, D.; Han, Z.; Lei, J.; Niu, Y.; Liu, H.; Shin, S.; Liu, C.; Guo, Z. Core-shell structured BN/SiO2 nanofiber membrane featuring with dual-effect thermal management and flame retardancy for extreme space thermal protection. *Sci. Bull.* **2025**, *70*, 722.
48 Ouyang, S.; Jiang, Q.; Wan, Y.; Qu, X.; Yu, Z.; He, H.; Wang, J. High thermal buffer and radiative cooling sodium alginate-based Janus aerogel enables multi-scenario thermal management for firefighting clothing. *Int. J. Biol. Macromol.* **2024**, *275*, 133533.
49 Cai, W.; Wang, J.; Wang, W.; Li, S.; Rahman, M. Z.; Tawiah, B.; Ming, Y.; Zhou, X.; Xing, W.; Hu, Y.; Zhu, J.; Fei, B. Colored radiative cooling and flame-retardant polyurethane-based coatings: selective absorption/reflection in solar waveband. *Small* **2024**, *20*, 2402349.
50 Bozdoğan, A.; Aksakal, B.; Denktaş, C.; Salt, Y. Prestretching effect and recovery process of polyvinyl alcohol film crosslinked with tartaric acid. *J. Appl. Polym. Sci.* **2020**, *137*, 49421.
51 Rajawasam, C. W.; Dodo, O. J.; Weerasinghe, M. S. N.; Raji, I. O.; Wanasinghe, S. V.; Konkolewicz, D.; Watuthanthrige, N. D. A. Educational series: characterizing crosslinked polymer networks. *Polym. Chem.* **2024**, *15*, 219.
52 Sheng, L.; Ren, J.; Hua, K.; Li, H.; Feng, Y.; Deng, M. The enhancement of mechanical properties of P84 hollow fiber membranes by thermally annealing below and above Tg. *J. Membrane. Sci.* **2020**, *595*, 117580.
53 Farooq, A. S.; Song, X.; Wei, D.; Liu, L.; Zhang, P. A bioinspired hierarchical gradient structure to maximize resilience and enhanced cooling performance in polymeric radiative cooling coatings. *Mater. Today. Energy* **2024**, *45*, 101666.
54 Du, Y.; Wang, W.; Mei, J.; Zhang, L. Silica-bridged inorganic-organic hybrid membrane for efficient daytime radiative cooling. *Chem. Eng. J.* **2024**, *485*, 149976.
55 Cai, C.; Chen, F.; Wei, Z.; Ding, C.; Chen, Y.; Wang, Y.; Fu, Y. Large scalable, anti-ultraviolet, strong cellulose film with well-defined dual-pores for longtime daytime radiative cooling. *Chem. Eng. J.* **2023**, *476*, 146668.
56 Yang, F.; Chai, R.; Zhang, J. Construction of a multi-scale microporous structure in EVA matrix toward passive cooling roofs. *J. Phys. Chem. Solids* **2023**, *178*, 111358.